ACSNANO

www.acsnano.org

ARTICLE

Ligand Addition Energies and the Stoichiometry of Colloidal Nanocrystals

Michael Sluydts,[†] Kim De Nolf,[‡,¶] Veronique Van Speybroeck,[†] Stefaan Cottenier,[*,†,§] and Zeger Hens[*,‡,¶]

[†]Center for Molecular Modeling, Ghent University, 9000 Gent, Belgium

[‡]Physics and Chemistry of Nanostructures, Ghent University, 9000 Gent, Belgium

[¶]Center for Nano and Biophotonics, Ghent University, 9000 Gent, Belgium

[§]Department of Materials Science and Engineering, Ghent University, 9000 Gent, Belgium

Supporting Information

ABSTRACT: **Experimental nonstoichiometries of colloidal nanocrystals such as CdSe and PbS are accounted for by attributing to each constituent atom and capping ligand a formal charge equal to its most common oxidation state to obtain an overall neutral nanocrystal. In spite of its apparent simplicity, little theoretical support of this approach—called here the oxidation-number sum rule—is present in the current literature. Here, we introduce the ligand addition energy, which we define as the energy gained or expended upon the transfer of one ligand from a reference state to a metal-rich solid surface. For the combination of CdSe, ZnSe and InP with either chalcogen, halogen or hydrochalcogen ligands, we compute successive ligand addition energies using *ab initio* methods and determine the thermodynamically stable surface composition as that composition where ligand addition turns endothermic. We find that the oxidation-number sum rule is valid in many situations, although exceptions occur for each material studied, most notably when exposed to small oxidative ligands. In the case of InP, however, violations are more severe, extending toward the entire chalcogen ligand family. In addition, we find that electronegativity rather than chemical hardness is a reasonable predictor for ligand addition energies, with the most electronegative ligands yielding the most exothermic addition energies. Finally, we argue that the ligand addition energy will be a most useful quantity for future computational studies on the structure, stability and reactivity of nanocrystal surfaces.**

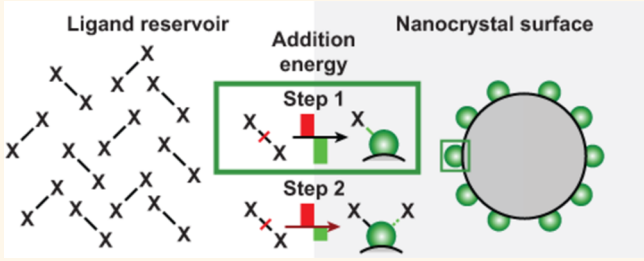

KEYWORDS: *nanomaterials, surface chemistry, quantum dots, nonstoichiometry*

Colloidal nanocrystals (NCs) are in many respects a hybrid class of nanomaterials. When synthesized using precision methods such as hot injection or heating up in apolar solvents, they consist of an inorganic core, typically 2−20 nm in diameter, capped by a monolayer of organic ligands.[1−3] Whereas the inorganic core has a crystal structure that closely resembles that of the bulk counterpart, the binding of ligands to the nanocrystal surface can be well described using coordination-chemistry concepts such as the covalent bond classification scheme.[4−7] In recent years, various detailed studies on binary semiconductor nanocrystals such as CdSe, CdTe, PbSe and PbS have shown that their stoichiometry differs from the 1:1 cation to anion ratio of the bulk counterpart.[8−11] Depending on their size, cation:anion ratios of up to 3:2 were found that could be attributed to a cation enrichment at the nanocrystal surface.[8] In parallel, it was demonstrated that these nanocrystals are terminated by ligands such as carboxylates,[9,10] phosponates[4,12,13] or thiolates[4] that have in the exemplary case of carboxylate-coordinated CdSe nanocrystals a well-defined 2:1 stoichiometry relative to the excess cations.[9] As a result, the generic chemical formula $[CdSe]_m(CdX_2)_n$ has been put forward for this class of nanocrystals, where the parts in square and round brackets denote the stoichiometric inorganic core and the surface termination by CdX_2 complexes, respectively.[5,14]

Within the covalent-bond classification, X-type ligands are coordinating agents that provide in their neutral form one electron to form a nanocrystal-ligand bond.[15] This applies for example to carboxylates, where the corresponding carboxyl radical indeed classifies as an X-type ligand. As a result, the CdX_2 surface termination can be explained by both X-type ligands taking one electron from the excess Cd, leaving the latter in its typical +2 oxidation state and turning the X-type

Received: November 4, 2015
Accepted: December 29, 2015
Published: December 29, 2015

DOI: 10.1021/acsnano.5b06965
ACS Nano 2016, 10, 1462−1474

ligand in its corresponding anion. This leads to a comprehensive picture of the nanocrystal composition where the overall charge neutrality of colloidal nanocrystals in apolar solvents is accounted for by attributing to each of its constituent atoms a formal charge equal to its characteristic oxidation state, such as +2 for Cd, −2 for Se and −1 for the X-type ligand-turned-anion.[5] This approach, which we will refer to as the oxidation-number sum rule or the sum rule in short, was supported by additional studies on, *e.g.*, PbS nanocrystals. Even if these had a more complex surface termination by oleate and chloride moieties, the overall nonstoichiometric nanocrystal composition again leads to a zero oxidation-number sum when attributing a formal charge of −1 to all X-type ligands.[10] The interplay between charge balancing and the stoichiometry of colloidal nanocrystals is further confirmed by the finding that a second class of nanocrystals exists that combine a stoichiometric composition with dative, L-type ligands—denoted as $[CdSe]_m(L)_n$ in the case of CdSe.[7,14] Since these bring in themselves the two electrons to form the ligand-nanocrystal bond, they can be attributed a formal charge of 0 and a zero oxidation-number sum is obtained by simply summing up the oxidation numbers of the atoms constituting the inorganic core. The oxidation-number sum rule is demonstrated for both X- and L-type adsorption in Figure 1.

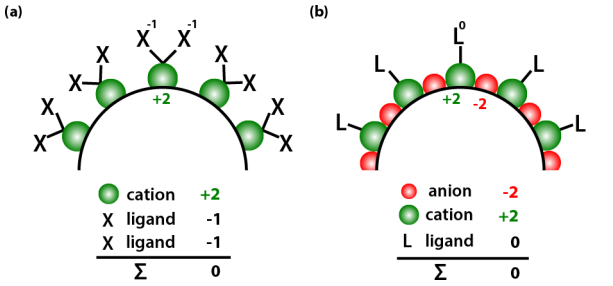

Figure 1. Bonding mechanisms of (a) X-type ligands on an excess surface and (b) L-type ligands on a stoichiometric surface.

With its comprehensive description of stoichiometry, ligand binding and charge neutrality, the delineation of nanocrystal classes has led to versatile and powerful ligand-exchange reactions and more realistic nanocrystal simulations. The latter involve for example density-functional theory (DFT) calculations on either periodic or cluster models by which the stability of a surface composition or the reaction enthalpy of different ligand exchange processes can be assessed.[16,17] Although extremely useful, these approaches take the experimental nanocrystal stoichiometry as a starting point and leave aside the more fundamental question as to what nanocrystal stoichiometry is thermodynamically the most favorable. In essence, this concerns the validity of the oxidation-number sum rule, which accounts for charge neutrality of the entire nanocrystal by attributing to each constituent a formal charge equal to its characteristic oxidation state. Whereas this is most likely a valid approach for ionic crystals, it is more questionable for nanocrystals of more covalent compounds or pure substances, especially if the constituting atoms can take different oxidation states.

Here, we introduce a computational approach to investigate ligand/nanocrystal binding and the preferred nanocrystal stoichiometry based on the ligand addition energy, which we define as the energy change upon adsorption of one additional ligand from a reference state to the nanocrystal surface. The value of this framework is assessed by a study on different ligand/semiconductor combinations using periodic DFT calculations, focusing on small inorganic ligands with well-defined oxidation states such as halogens/halides or chalcogens/chalcogenides. For the systems studied, it appears that trends in ligand addition energies largely reflect ligand electronegativity rather than, *e.g.*, a matching of chemical hardness between ligand and excess metal as predicted by hard−soft acid−base theory. Moreover, we find that more ionic materials such as CdSe and ZnSe indeed mostly show endothermic ligand addition energies once the nanocrystal stoichiometry exceeds that predicted by the oxidation-number sum rule. Nevertheless, exceptions occur for small electronegative ligands since these tend to oxidize both the excess metal and the surface anions. In the case of InP, these violations are more severe, with Z-type chalcogen ligands clearly defying the sum rule. This makes the extension of the oxidation-number sum rule to materials other than the widely studied II−VI and IV−VI materials far from trivial and even for these materials care should be taken. The theoretical analysis of ligand addition energies as introduced here—either using periodic or cluster models—will provide the starting point to understand the surface termination of nanocrystals also in these more complex cases. Moreover, the surface composition where ligand addition energies turn endothermic corresponds to thermodynamic equilibrium between a nanocrystal and a given ligand reservoir. Ligand addition energies are therefore most useful quantities to analyze and understand the stability of nanocrystals upon exposure to, *e.g.*, oxygen, water or specific precursors during more involved synthetic procedures. We thus conclude that the ligand addition energy as introduced here constitutes a highly valuable and versatile concept for the computational analysis of the stability and reactivity of nanocrystals and nanocrystal surfaces.

BACKGROUND

Ligand Addition Energy. The ligand addition energy can be considered the energetic cost of adding a ligand from its reference state to the nanocrystal surface. This process is represented schematically in Figure 2(a) for the case of Cl adsorption on $[CdSe]Cd_n$, *i.e.*, a CdSe NC with n excess Cd atoms. Here, the ligand reference state is taken as the corresponding ground-state dimeric crystal at 0 K. The diagram shows the sequential addition of Cl ligands to the surface from the reference reservoir. In each adsorption step a ligand addition energy E^k_{add} is expended, representing the energetic cost of adding the k^{th} ligand from the reservoir and breaking the corresponding Cl_2 bond. Within this framework, the ligand addition energy E^k_{add} can be defined as

$$E^k_{add} = E^k_{surf} - E^{k-1}_{surf} - \mu_{lig} \quad (1)$$

Here, E^k_{surf} represents the total energy of the nanocrystal with k ligands adsorbed, while μ_{lig} is the chemical potential of one ligand unit in the reference state. Given the tendency of the nanocrystal and the reservoir to minimize their total energy, ligands will be added to the nanocrystal surface from the reservoir as long as E^k_{add} remains exothermic. For endothermic ligand addition energies, it becomes energetically more favorable for the entire system if the ligands remain in or return to their reference state. This implies that the most stable surface composition will be determined by a ligand:excess Cd

DOI: 10.1021/acsnano.5b06965
ACS Nano 2016, 10, 1462−1474

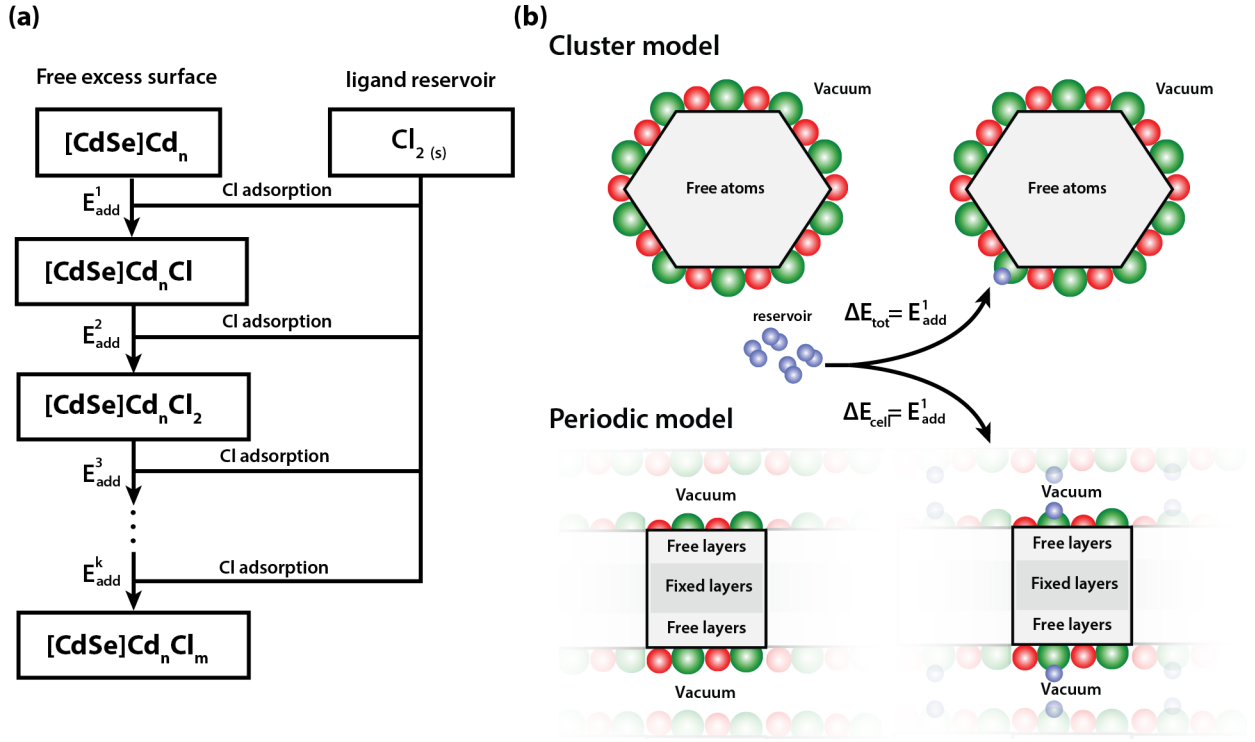

Figure 2. (a) Stepwise schematic demonstrating the ligand addition energy for Cl adsorption on excess Cd (b) Corresponding surface configurations in cluster and periodic models.

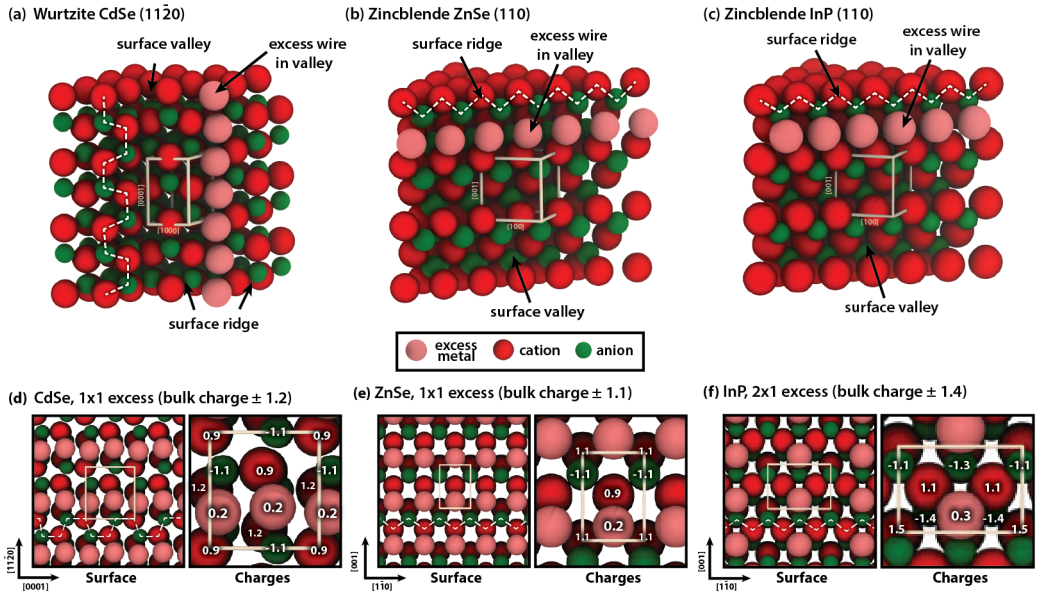

Figure 3. Cleavage of (a) a wurtzite CdSe crystal at the (11$\bar{2}$0) plane, (b) a zinc blende ZnSe crystal at the (110) plane and (c) a zinc blende InP crystal at the (110) plane. In all three cases, a combination of the pristine and the relaxed excess surface is shown with the dashed line indicating the chairlike or zigzag like ordering of cations and anions characteristic of the (11$\bar{2}$0) wurtzite or (110) zinc blende lattice, respectively. Top view and corresponding Hirschfeld-I charges of (d) the relaxed excess (11$\bar{2}$0) wurtzite CdSe surface, (e) the relaxed excess (110) zinc blende ZnSe surface and (f) the relaxed excess (110) zinc blende InP surface.

ratio of *m*:*n*, where *m* is the last exothermic ligand addition energy. Hence this step plays the pivotal role in determining the thermodynamically preferred nanocrystal stoichiometry.

Periodic *vs* Cluster Models. Determination of ligand addition energies requires both a way of representing the nanocrystal surface as well as a means to calculate its energy. These energy calculations are done through DFT, the methodology of which is explained in the Methods section. This section will focus on the creation of a geometric representation of the surface. Representing the surface is typically done by means of either a periodic or a cluster model. In a periodic model a facet of the nanocrystal surface is represented by an infinitely expanded flat slab. This slab is constructed through the three-dimensional periodic repetition of a unit cell, containing the minimally symmetric unit necessary to represent the slab along with a fixed vacuum gap

DOI: 10.1021/acsnano.5b06965
ACS Nano 2016, 10, 1462−1474

separating it from its periodic image. When either a lower symmetry or defect density, *e.g.*, excess atoms or ligands, is necessary, a larger supercell can be created by extending the unit cell along its lattice vectors.[18−20] A cluster model makes no such use of symmetry and represents the nanocrystal as a whole, with different parts of the surface corresponding to different bulk cleavage planes.[21−27]

Although a cluster model could be considered more realistic, it is also significantly more complex. This is demonstrated in Figure 2(b) where the addition of a single ligand from the reservoir is schematically demonstrated for both models. The presence of edges and different facets on a cluster model leads to various, inequivalent adsorption sites. This greatly increases the difficulty of finding the lowest-energy configuration of the total system and can introduce spurious variations in the ligand addition energy. The size of a realistic system also makes it difficult to perform simulations at a sufficiently high accuracy level, limiting the configurational space that can be explored. In a periodic model the ligand:cation ratio is increased in larger steps, with identical interactions ensured between all ligands and excess atoms on the surface. This allows both size and accuracy of the system to be tightly controlled and negates spurious energetic effects which do not provide any information about the interactions of interest. A periodic model is thus considered the optimal choice for use within this study, which aims at screening a number of ligands and materials to explore the usefulness of the ligand-addition energy framework for describing ligand binding and retrieving the preferred nanocrystal stoichiometry.

RESULTS

Systems Studied. Slab models have been created for CdSe, ZnSe and InP. CdSe and ZnSe represent chemically similar ionic crystals, while InP is chosen as an example of a more covalent crystal with a less electronegative anion. All materials have been modeled in their most common phase, *i.e.*, wurtzite for CdSe and zinc blende for ZnSe and InP. For both crystal types, either the $(11\bar{2}0)$ or the (110) surfaces were selected for calculating ligand addition energies since these are low-index surfaces with a sufficiently low surface energy to commonly be present on the nanocrystal surface.[19,28−30] The excess surfaces were then created by adding the relevant metal atoms, with no explicit charge imposed on the ligand-free excess surface as adsorption takes place from a neutral ligand reservoir. This results in an adsorbed system which remains globally neutral, but local effective charges are automatically acquired when energetically favorable. In a final step, DFT is used to find the relaxed excess surface, while the center of the slab model remains constrained to the bulk geometry.

Figure 3a shows a CdSe $(11\bar{2}0)$ surface as cleaved from the bulk. In the figure, the dashed line indicates the chairlike chains of Cd and Se atoms parallel to the [0001] direction that characterize the pristine $(11\bar{2}0)$ surface. Rather then occupying the corresponding bulk positions, we find that the excess Cd atoms form a wire-like ordering in the valleys separating two Cd−Se chairlike chains. This ordering is represented in the top view image shown in Figure 3d, where both the Cd−Se chairlike chain and the wire of excess atoms can be readily distinguished. In addition, the figure represents the surface unit cell and the Hirschfeld-I charges calculated for the surface and excess atoms. The latter will be referred to simply as charges in the remainder of the text. They indicate that the excess Cd remains almost uncharged after adsorption, acquiring a charge of only +0.2 mainly by reducing the charge on the surface Cd. Similar cleavage and top views of the (110) surface of ZnSe and InP cleaved are given in Figures 3b, 3e and 3c, 3f, respectively. Note that in the case of InP, extended unit cells 1 × 2 (see Figure 3f) and 2 × 1 (see Supporting Information S5) have been used to ensure similar ligand densities for all systems after ligand addition (see Table 1). The zinc blende (110) plane features characteristic zigzag chains of cations and anions parallel to the [110] direction as indicated by the dashed lines. Again, the excess atoms relax in a wire-like configuration in between these zigzag chains, although the positioning of the excess atoms relative to the surface atoms is different for both materials. Similar to the excess Cd, also the excess Zn and In only acquire a small positive charge. A more detailed discussion of these relaxed excess surfaces can be found in section S1 of the Supporting Information.

Table 1. Studied Nanocrystal Surfaces

	CdSe	ZnSe	InP
structure	WZ	ZB	ZB
surface	$(11\bar{2}0)$	(110)	(110)
surface area (nm × nm)	0.71 × 0.76	0.41 × 0.57	2 × 1: 8.3 × 5.9 1 × 2: 4.1 × 11.7
cation density (nm^{-2})	3.7	4.3	2.1
stoich Z density (nm^{-2})	3.7	4.3	3.1
Stoich X density (nm^{-2})	7.3	8.6	6.2

On each of the excess surfaces 12 ligand species are introduced, grouped into three sets:

- Chalcogens (Z): O, S, Se and Te
- Hydrochalcogens (X = ZH): OH, SH, SeH and TeH
- Halogens (X): F, Cl, Br and I.

Within each set chemically similar ligands are studied to isolate effects of properties such as size, electronegativity and chemical hardness on the ligand addition energy. As reference state for the chemical potential the energy of the corresponding 0 K ground-state crystals is chosen which is calculated using DFT. For species like O and halogens these are weakly interacting dimeric crystals, while S, Se and Te condense into true bulk solids. Hydrochalcogen reference states are obtained by combining chalcogen reference states with the lowest-energy H_2Z crystal for each species (Z = O, S, Se, Te) through the following reaction:

$$H_2Z + \frac{1}{2}Z_2 \rightarrow 2ZH \tag{2}$$

corresponding to a chemical potential of

$$\mu_{ZH} = \frac{1}{2}\left(\mu_{H_2Z} + \frac{1}{2}\mu_{Z_2}\right) \tag{3}$$

These can then be used to determine the ligand addition energy in each case.

Ligand Addition Energies, General Overview. For all combinations of ligands and materials, ligand addition energies have been calculated by progressively adding ligands to the respective reconstructed excess surfaces. After energy minimization through a screening of potential positions and the concomitant geometric relaxation, the corresponding ligand addition energy has been calculated from the lowest energy state found using eq 1. The resulting nine graphs are shown in Figure 4, where the ligand species can always be found on the horizontal axis, moving downward through the periodic table

DOI: 10.1021/acsnano.5b06965
ACS Nano 2016, 10, 1462−1474

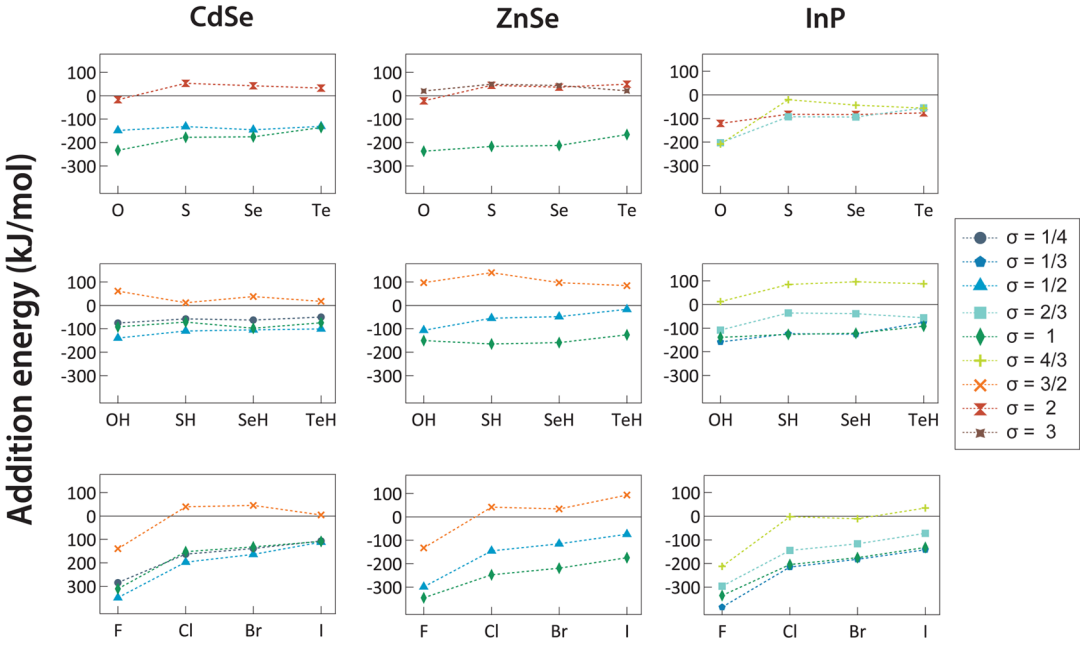

Figure 4. Ligand addition energy (in kJ/mol) for the different combinations of ligand set and material. Rows correspond to the ligand family while materials are represented by the columns. Exothermic addition energies correspond to adsorbed states. Stoichiometry ratio varies by color with blue to red corresponding to sub and superstoichiometric. Available σ is dependent on the simulated cell.

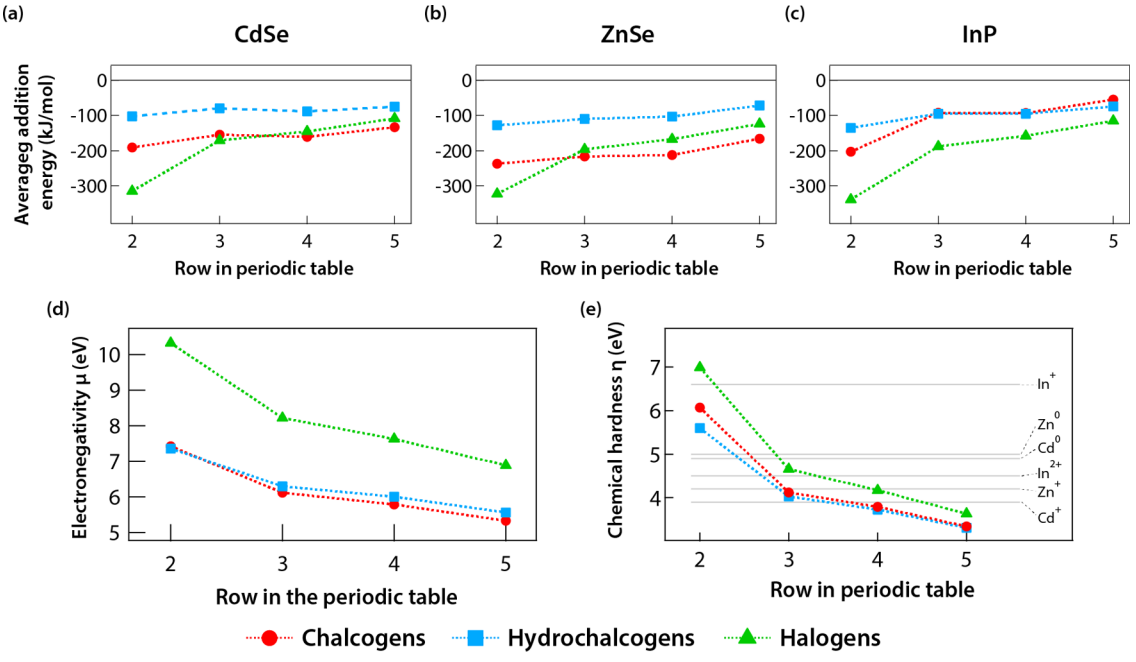

Figure 5. Average addition energy (in kJ/mol) for $\sigma \leq 1$ on (a) CdSe, (b) ZnSe, (c) InP. Evolution of (d) Mulliken electronegativity and (e) Pearson's chemical hardness (in eV) for chalcogen, hydrochalcogen and halogen ligands. Hardness values for Cd^{2+}, Zn^{2+}, In^{3+} and In^{0} have been omitted as they fall outside of the plotted range of ligand hardness.

from left to right. Within each graph, each individual curve represents the addition energy for a specific surface stoichiometry ratio σ as obtained after the considered ligand addition step:

$$\sigma = \frac{\text{adsorbed ligand density}}{\text{expected ligand density}} \quad (4)$$

This definition makes the expected stoichiometry as determined by the oxidation-number sum rule correspond to a stoichiometry ratio $\sigma = 1$, while $\sigma > 1$ and $\sigma < 1$ represent sub- and supra-stoichiometric surfaces, respectively.

Before using the ligand addition energy to assess nanocrystal stoichiometry, however, it is useful to first analyze its magnitude and possible trends in either of the three ligand series. For this purpose, Figure 5a represents the average value of the different addition energies for all $\sigma \leq 1$ compositions. First of all, not only the averages but effectively all of these addition energies are exothermic, meaning that ligand addition is always favorable up to the stoichiometry predicted by the sum rule. Moreover,

DOI: 10.1021/acsnano.5b06965
ACS Nano 2016, 10, 1462−1474

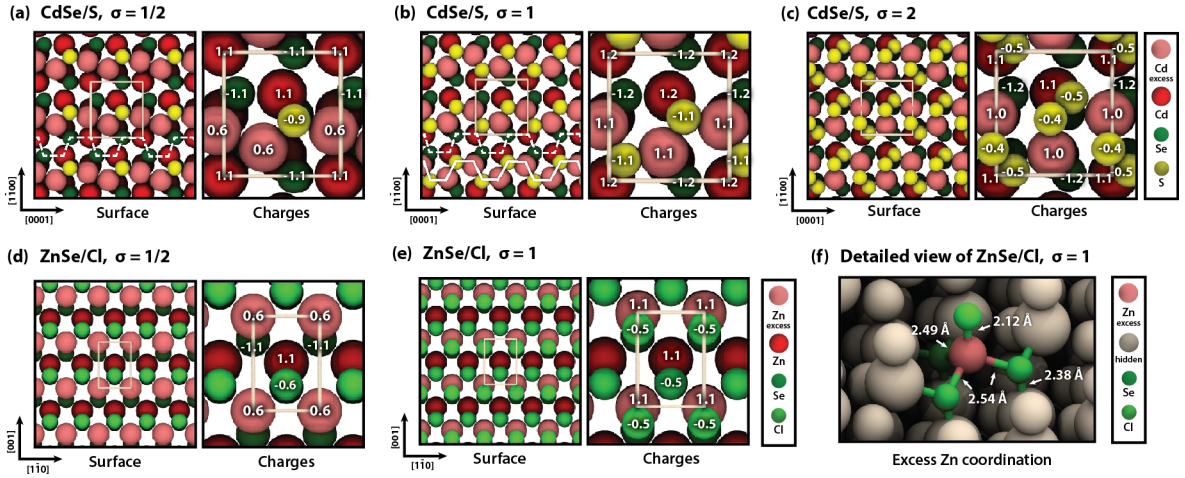

Figure 6. (Upper panels) Top view on the CdSe (11$\bar{2}$0) surface subjected to progressive sulfur addition with occupation σ increasing from (a) 0.5 to (b) 1 and (c) 2. (Lower panels) Top view on the ZnSe (110) surface subjected to progressive chlorine addition with occupation σ increasing from (d) 0.5 to (e) 1. In (a) and (b), the full and dashed lines represent the typical chair (CdSe (11$\bar{2}$0)) or zigzag (ZnSe (110)) ordering of anions and cations in the surface and the excess layer, respectively. A detailed view of the local tetrahedral coordination of the excess atom from (e) is shown in (f).

especially for the halogens and the hydrochalcogens, it can be seen that both the absolute value of the addition energy and its trend with period number are highly similar. Halogens always exhibit the most exothermic addition energies and do so for all systems; the addition energy becomes less exothermic with increasing period. The chalcogens show a somewhat larger variation, with more exothermic addition energies in the case of ZnSe and less exothermic for InP, yet even then differences remain small and especially the tendency of the addition energy to become less exothermic with increasing period persists.

To understand the chemical factors determining the addition energies, Figure 5b and c show the electronegativity μ and chemical hardness η of the different ligands studied, two widely used chemical properties that we quantify using the following definitions (IP: ionization potential; EA: electron affinity):[31−33]

$$\mu = \frac{\mathrm{IP} + \mathrm{EA}}{2} \tag{5}$$

$$\eta = \frac{\mathrm{IP} - \mathrm{EA}}{2} \tag{6}$$

Both quantities can be determined *ab initio* at high accuracy due to the limited size of the simulated systems and the numbers we calculate closely match tabulated values where available.[34,35]

Hardness is the central quantity in hard−soft acid−base (HSAB) theory,[34−36] which tends to explain strong bonding affinity between metal ions and ligands by the principle of hardness matching, where hard or soft ligands preferably bind to hard or soft ions, respectively.[34−36] For this reason, we have added to Figure 5c the chemical hardness of Cd, Zn and In and their ions. Apart from Cd^{2+}, Zn^{2+}, In^{3+} and In^{+}, where only the latter is of relevance to the systems studied given the bulk charges of +1.2, + 1.1 and +1.4 on the cations in CdSe, ZnSe and InP, respectively−these metals and their ions have a hardness in the range 4−5 eV. This gives a strong hardness mismatch with period 2 ligands and a reasonable overlap with period 3−4 ligands. Translating this hardness-matching into addition energy trends however does not match even the simplest observations in Figure 5a—the similarly strong preference of CdSe, ZnSe and InP for F—and suggests great care should be taken when trying to apply HSAB to nanocrystal surfaces. This theory inherently assumes interaction with an isolated ion and neglects the effects the surface may have on the ligand bonding, either through geometric effects such as sterical hindrance or by altering the identity of the ion by delocalizing the charge.

Figure 5c indicates that the calculated electronegativity monotonously decreases with increasing period within each ligand set. Especially for the halogens and the hydrochalcogens, this trend correlates well with the addition energy, with the more electronegative halogens systematically yielding addition energies with higher absolute values. As the difference in Mulliken electronegativity (eq 6) between two binding moieties largely corresponds to the ionic contribution to the two-electron bond strength, this correspondence between electronegativity and addition energy indicates that ligand addition involves the formation of mainly ionic bonds for the systems studied. The apparently deviating behavior of the chalcogens, which feature more exothermic addition energies than the hydrochalcogens while having similar electronegativity, can be understood within this picture since for these ligands binding involves the formal transfer of 2 electrons instead of 1 to the ligand. This makes that oxygen typically features a high addition energy, second only to fluorine, even if its Mulliken electronegativy is comparable to that of bromine and iodine. Hence, it appears that opposite from hardness, electronegativity largely captures the variation of addition-energy with period number.

To facilitate the assessment of nanocrystal stoichiometry, all addition energies in Figure 4 have been color-encoded depending on the corresponding stoichiometry ratio σ, where colors vary from blue to red for sub- to suprastoichiometric addition energies and the expected σ = 1 stoichiometry has been colored green. It can thus be seen that for a large range of material/ligand combinations, the oxidation sum rule applies, with addition energies becoming endothermic once σ exceeds one. Exceptions occur either with specific ligands or materials, where small electronegative ligands such as F and O yield exothermic suprastoichiometric addition energies for all materials studied while InP features exothermic suprastoichio-

DOI: 10.1021/acsnano.5b06965
ACS Nano 2016, 10, 1462−1474

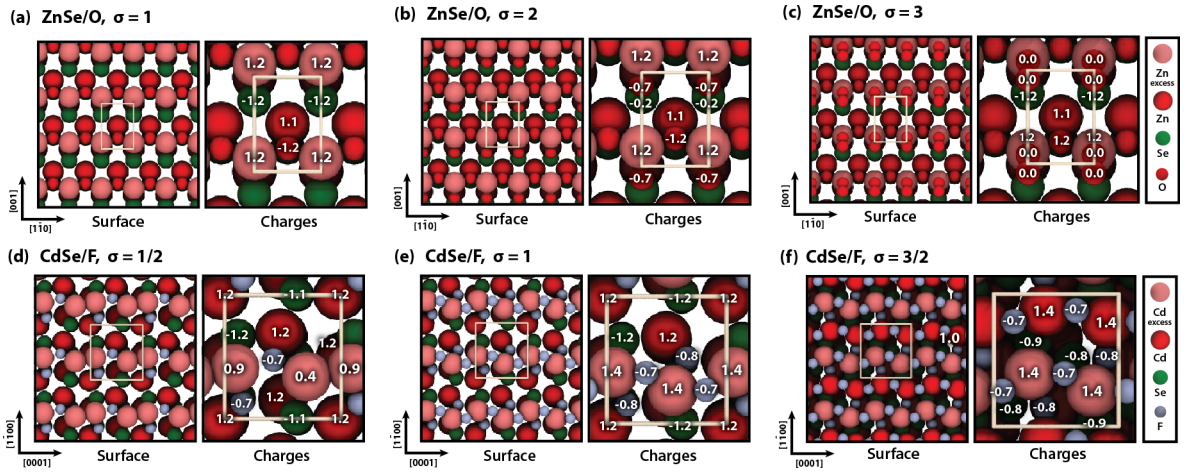

Figure 7. (Upper panels) Top view on the ZnSe (110) surface subjected to progressive oxygen addition with occupation σ increasing from (a) 1 to (b) 2 and (c) 3. (Lower panels) Top view on the CdSe (11$\bar{2}$0) surface subjected to progressive fluorine addition with occupation σ increasing from (d) 1/2 to (e) 1 and (f) 3/2.

metric addition energies for all chalcogens. Remarkably, these ligands are capable of adsorbing to double the expected stoichiometry ratio without incurring any endothermic addition energies. This suggests the observed trends and deviations are both ligand and material-dependent and are affected by the configuration of the adsorbate-covered surface.

Sum-Rule Compliant Material/Ligand Combinations. Of all 36 material/ligand combinations studied, 25 comply with the oxidation number sum rule in the sense that the addition energy is exothermic as long as $\sigma \leq 1$ and turns endothermic when σ exceeds unity. This includes the addition of all hydrochalcogens and all halogens bar fluorine to the three semiconductors studied and the addition of all chalcogens bar oxygen to CdSe and ZnSe. Rather than discussing all these 25 systems separately, we consider here a few representative examples and present surface morphologies at different stoichiometry ratios of all other systems in the Supporting Information.

Figure 6a–c represents different steps of the progressive addition of sulfur to a CdSe (11$\bar{2}$0) surface. Due to the size of the CdSe supercell, which contains two excess Cd atoms, the substoichiometric step σ = 0.5 can be simulated in addition to the stoichiometric σ = 1 step. Looking first at this intermediate σ = 0.5 stoichiometry ratio—which we will systematically indicate as the CdSe/S, σ = 0.5 surface—Figure 6a shows that the added S is inserted between two excess Cd atoms, thus breaking the Cd wire formed on the relaxed excess CdSe (11$\bar{2}$0) surface into a sequence of Cd dimers separated by sulfur atoms. Moreover, the added S atoms acquire a charge of −0.9 at the expense of an increasingly positive charge of +0.6 on the excess Cd atoms, which can be seen as an oxidation of the excess Cd atoms by the S ligands. Both the trends of surface reorganization and oxidation of the excess Cd persist upon further increasing the stoichiometry ratio to σ = 1. On the CdSe/S, σ = 1 surface, the added S and the excess Cd form the chairlike chains characteristic of the CdSe (11$\bar{2}$0) surface (see full white lines in Figure 6b), while taking surface positions in close agreement with the Cd and S positions in bulk wurtzite CdSe. In addition, the charge on the excess Cd and the added S further increases to +1.1 and −1.1, respectively, figures almost equal to the respective +1.2 and −1.2 charges on Cd and Se atoms in bulk CdSe. Further addition of sulfur to the CdSe surface leads to the formation of disulfide bridges on the CdSe/S, σ = 2 surface—reducing the charge on each sulfur atom—between the excess Cd atoms, which still occupy sites close to the corresponding bulk position. This process comes with an endothermic addition energy, such that sulfur addition stops at a σ = 1 stoichiometry ratio where a close to epitaxial CdS monolayer is formed on the CdSe surface.

A similar picture emerges in the case of ZnSe/Cl, for which surface geometries are represented in Figures 6d–f. Here, both an intermediate σ = 0.5 and a final σ = 1 stoichiometry ratio can be studied since each ZnSe unit cell contains one excess Zn atom, yet 2 Cl atoms per unit cell are needed to reach a σ = 1 excess. As shown in Figure 6d, the original reconstruction of the excess ZnSe (110) surface leading to Zn wires in between the characteristic Zn–Se zigzag chains is already undone on the ZnSe/Cl, σ = 0.5 surface. The excess Zn atoms move to adsorption sites closely corresponding to bulk positions while the Cl ligands adsorb on sites that are occupied by Se in bulk ZnSe. As a result, next to the Zn–Se zigzag chains, the excess surface now features Zn–Cl chains connecting excess Zn and added Cl. In addition, the added Cl mainly oxidized the excess Zn, resulting in charges of +0.6 and −0.6 on the excess Zn and the Cl ligands, respectively. Again, both trends persist when the stoichiometry ratio is increased to σ = 1. On the ZnSe/Cl, σ = 1 surface, the added ligands complete the 4-fold tetragonal coordination of the excess Zn atoms (Figure 6f)—just like Se does in bulk ZnSe—and further oxidize the excess Zn whose charge of +1.1 corresponds to that on Zn atoms in bulk ZnSe.

As shown in the Supporting Information (section S5), adsorption of ligands on sites closely corresponding to lattice positions occupied by the anions in the bulk crystal is observed at σ = 1 for all material/ligand combinations that comply with the oxidation-number sum rule except OH. Even for halogen addition to InP, the excess In eventually acquires a tetragonal coordination involving one surface P atom and 3 added ligands. One remarkable observation here is the occurrence of chemical transformations of the ligands in the case of hydrochalcogen addition. For instance upon addition of SeH to CdSe, the stable σ = 1 configuration consists in the separate adsorption of Se and H_2Se rather than two SeH moieties. However, even in this case, both Se atoms still occupy positions corresponding to bulk Se sites (see Supporting Information S2).

DOI: 10.1021/acsnano.5b06965
ACS Nano 2016, 10, 1462–1474

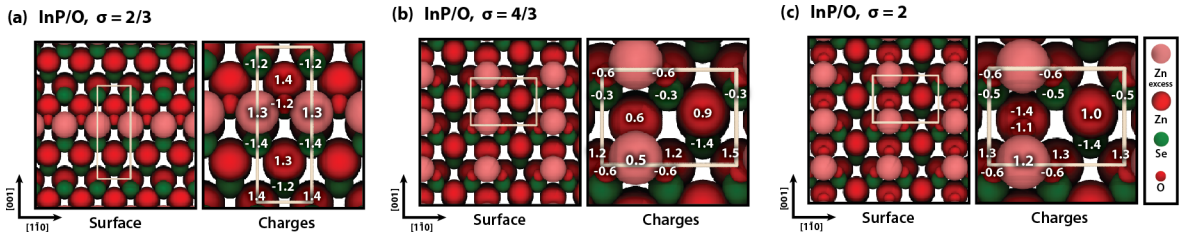

Figure 8. Top view on the InP (110) surface subjected to progressive oxygen addition with occupation σ increasing from (a) 2/3 to (b) 4/3 and (c) 2.

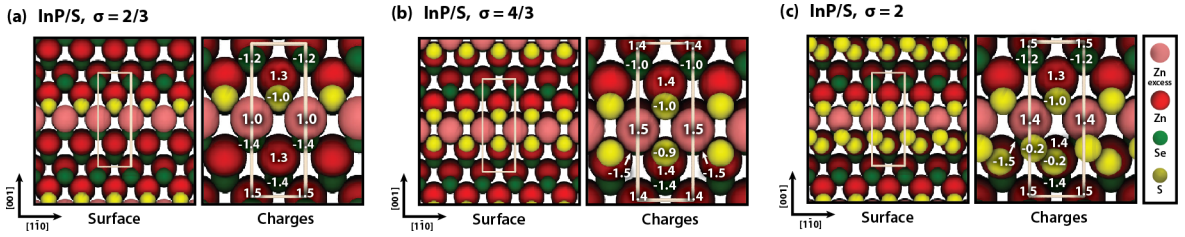

Figure 9. Top view on the InP (110) surface subjected to progressive oxygen addition with occupation σ increasing from (a) 2/3 to (b) 4/3 and (c) 2.

F and O, Sum-Rule Defiant Ligands. Figure 4 shows that oxygen and fluorine addition to CdSe, ZnSe and InP remains thermodynamically favorable above the $\sigma = 1$ limit predicted by the oxidation-number sum rule. According to Figure 5, these are also the most oxidative halogen or chalcogen ligands yielding in general the most exothermic addition energies up to the $\sigma = 1$ excess. To illustrate the general rules that apply to these suprastoichiometric material/ligand combinations involving F and O, we will again present a few representative examples while an exhaustive overview is given in the Supporting Information (see section S5).

Figure 7a–c shows top views of the ZnSe/O surface where the stoichiometry ratio is systematically increased from $\sigma = 1$ to $\sigma = 3$. Since the ZnSe supercell used contains a single excess Zn atom only, oxygen addition is only possible in these coarse steps. The surface geometry found for the ZnSe/O, $\sigma = 1$ surface resembles the arrangement of excess atoms and ligands typically found for sum-rule compliant systems. The original reconstruction of the excess surface is undone; excess Zn atoms have shifted close to the positions they would occupy in a new bulk layer; O ligands adsorb on surface sites more or less corresponding to Se bulk positions and charges on excess Zn are close to that on Zn in bulk ZnSe. Nevertheless, already now, the excess Zn atoms are shifted in the [001] direction relative to the bulk positions. Moreover, due to their small size, the oxygen atoms penetrate markedly in between two excess Zn atoms. In the same way, the oxygen atoms added to reach a $\sigma = 2$ stoichiometry ratio do not simply coordinate the excess Zn further. Rather, they insert between an excess Zn and a surface Se atom to form a Zn–O–Se bridge, thus breaking the original Zn–Se bond. According to the charges, this mainly leads to an oxidation of the surface Se, thus accounting for the suprastoichiometric surface configuration. This oxidation does however not persist upon further oxygen addition. Rather than further inserting between existing bonds, our computation shows that oxygen dimers are formed in a process that exhibits a slightly endothermic addition energy.

A similar picture but even more pronounced emerges in the case of CdSe/F, for which top views are shown in Figure 7d–f for a stoichiometry ratio increasing from $\sigma = 0.5$ to $\sigma = 1.5$. Also here, F addition breaks up the original reconstruction of the excess CdSe surface, yet the excess Cd atoms fail to reach the corresponding bulk position at a $\sigma = 1$ excess, nor do the F atoms adsorb at sites normally occupied by Se. Rather, several Cd–F–Cd bridges are formed leading to a pronounced oxidation of the excess Cd as attested by its charge of +1.4, which even exceeds the charge of +1.2 on Cd in bulk CdSe. Similar to ZnSe/O, the fluorine added to increase the stoichiometry ratio to $\sigma = 1.5$ starts interacting with the surface Se, again breaking Cd–Se bonds and replacing them by Cd–F–Se bridges. This inserted fluorine is not visible in the top view of the CdSe $(11\bar{2}0)$ surface shown in Figure 7f, yet its influence can be inferred from the reduced charge on the surface Se atoms, which drops from −1.2 to either −0.8 or −0.9.

As further demonstrated by the examples in the Supporting Information (section S5), the significant distortion of the surface as compared to an epitaxial continuation of the bulk lattice appears to be a general characteristic of O and F addition. As shown by the ZnSe/O example, this may lead to a suprastoichiometric surface composition, without implying by necessity the full oxidation of the bulk material. On the other hand, persistently exothermic addition energies with a progressive insertion of the ligands in between existing bonds may occur such as in the case of InP/O, where even at $\sigma = 8/3$ exothermic addition energies are retrieved (see Supporting Information S3).

InP, a Sum-Rule Defiant Material. In the case of chalcogen addition to InP, Figure 4 shows that ligand addition energies remain exothermic for a stoichiometry ratio exceeding unity for all chalcogens. This suggests that this material/ligand combination is systematically different from any ligand combination with CdSe and ZnSe or combinations of InP with halogens and hydrochalcogens.

Considering first the InP/O system, Figure 8 shows a top view on the InP (110) surface for a stoichiometry ratio progressively increasing from $\sigma = 2/3$ to $\sigma = 2$, which corresponds to the addition of 1 to 3 O atoms per supercell. The geometry of the InP/O, $\sigma = 2/3$ surface is comparable to that of the ZnSe/O, $\sigma = 1$ surface, with the excess In atoms

DOI: 10.1021/acsnano.5b06965
ACS Nano 2016, 10, 1462–1474

somewhat shifted along [001] relative to the bulk adsorption sites, the O atoms deeply inserted between adjacent excess In atoms and the charges indicating that O mostly oxidizes the excess In. For the InP/O, $\sigma = 4/3$ surface, the most stable geometry is found in a different supercell with the same excess In density (2×1 instead of 1×2). Here, the excess In atoms no longer occupy bulk adsorption sites and the added O atoms are inserted between In−P bonds, forming In−O−P bridges as shown before for ZnSe/O. This leads to a pronounced oxidation of the surface P, with charges dropping from −1.4 for bulk InP to only −0.3. Additional oxygen atoms form bridges between excess and surface In ($\sigma = 2$, Figure 8(c)), thereby further oxidizing the excess In as indicated by the increasing charge on the atom.

While O addition to InP follows similar rules as O and F addition to CdSe and ZnSe, a different picture emerges upon addition of other chalcogen atoms to InP. As shown in Figure 9, the InP/S, $\sigma = 2/3$ surface features a geometry similar to sum-rule compliant systems, where the excess In atoms are found close to the bulk In positions and the S ligands occupy bulk P positions while mainly oxidizing the excess In. Due to its symmetry, however, the InP $\sigma = 2/3$ surface still provides one free adsorption site per excess In. Adding one sulfur atom more to each supercell, a number already exceeding the expected $\sigma = 1$ stoichiometry, therefore leads to additional S adsorption on In−In bridge sites opposite from the sites already occupied at a $\sigma = 2/3$ excess. This configuration enables the added S to further oxidize both surface and excess In. Moreover, the pronounced size difference between In and P renders the adsorption sites in the second step more favorable as it makes the excess In screen the surface ligand from repulsion by surface P atoms. Further sulfur addition leads to a bridging of excess and surface In by S_2 dimers sharing the charge between the two S atoms.

DISCUSSION

The chemical formulas put forward in recent years for colloidal nanocrystals such as CdSe or PbS reflect the experimentally determined ratios between excess surface cations and surface ligands.[14] They follow a simple rule where each constituent atom is given a formal charge equal to its oxidation number to yield a nanocrystal with a total formal charge of zero, a procedure we called the oxidation-number sum rule. Here, we have analyzed nanocrystal stoichiometry by introducing the ligand addition energy E^k_{add} as the reaction energy for the addition of the k^{th} ligand from its reference state to the nanocrystal.

Using the fact that the last exothermic addition energy determines the nanocrystal stoichiometry, we thus assessed the validity of the oxidation-number sum rule for a range of nanocrystal/ligand combinations. In the case of more ionic binary crystals such as CdSe and ZnSe, our computations yield stoichiometries generally in line with the oxidation-number sum rule. Here, excess metal atoms and added ligands adsorb at positions close to bulk cation and anion positions, thus epitaxially extending the crystal lattice perpendicular to the cleavage plane, and binding mainly boils down to the oxidation of the excess metal by the added ligands. Exceptions occur with strongly oxidizing, small ligands such as fluorine and oxygen. These insert between both cation−cation and cation−anion bonds, thereby oxidizing also the anion and preventing the surface from extending the bulk crystal structure.

In the case of InP, not only do fluorine and oxygen give rise to similar deviations from the sum rule but also in the case of other chalcogen ligands, suprastoichiometric adsorption is systematically favorable. These deviations can be partially attributed to the lower electronegativity of both In and P, increasing the binding energy of strongly oxidizing ligands. Even so, ligands such as Cl and Br are still incapable of obtaining strongly exothermic addition energies above a $\sigma = 1$ stoichiometry ratio. This suggests that geometric considerations are at least of equal importance as electronegativity. Oxidizing the surface P leads to a weakening of the three In−P bonds that attach it to the crystal. Only in the case of F is the created F−P bond sufficiently strong to compensate this effect. Both for Cl and Br an addition energy of 0 is obtained with respect to the Cl_2 and Br_2 reservoir, suggesting the formed bond just compensates for the breaking of the Cl−Cl or Br−Br bond. Geometric effects are also the main reason for the strong oxidation sum-rule violations in the case of chalcogens. The desired ratio of Z ligands to excess In would be three Z^{2-} for every two In^{3+}. Such a configuration is not commensurate with a cubic lattice which prefers an even ratio. Available adsorption sites are determined by the lattice and deviations from an even ratio either lead to the inducement of geometric strain or require the breaking of bonds between the excess In and the surface. The result is the occupation of adsorption sites with suboptimal charge transfer and a lower addition energy. This leads to a more gradual oxidation of the surface, but with a larger final ligand density.

The example of InP gives a first indication that ligand addition energy is a concept whose possible use extends well beyond the analysis of nanocrystal stoichiometry. Nanocrystals kept under ambient conditions for example can be seen as exposed to ligand reservoirs of oxygen and/or water and also here, the ligand addition energy can be used to assess the influence of such an environment on the nanocrystals. The persistently exothermic addition energies for oxygen in the case of InP thus show that InP nanocrystals are prone to oxidation under ambient conditions, whereas this is less of a problem for CdSe and ZnSe whose oxygen addition energies become zero or becomes endothermic upon increasing stoichiometry ratio. This is in line with experimental findings, where oxidation is often problematic in the case of InP—even by reaction byproducts—whereas state-of-the-art CdSe and ZnSe nanocrystals can even be synthesized under ambient conditions.[37−40]

Their very synthesis constitutes another case where nanocrystals are exposed to a ligand reservoir. Considering the small inorganic moieties studied here, this may involve the deliberate exposure of core nanocrystals to reagents for growing an inorganic shell of materials such as ZnS, ZnSe or CdS or the unintentional exposure to impurities or reaction products. A notable example of the latter is the strong affinity of halides for the surface of CdSe nanocrystals—as confirmed here by their strongly exothermic addition energies—where a fine control over their concentration proved crucial for the reproducible synthesis of CdSe multipods and allowed for deliberate shape tuning.[41−43] For the formation of core/shell nanocrystals on the other hand, nanocrystals can be sequentially exposed to reagents providing the anions and the cations of the envisaged shell material in a so-called SILAR procedure, short for successive ion-layer adsorption and reaction.[44] Here, our study of the CdSe/S example confirms the experimental finding that in the case of CdS shell growth, reaction of sulfur with a Cd-rich nanocrystal results in a first CdS monolayer that grows

DOI: 10.1021/acsnano.5b06965
ACS Nano 2016, 10, 1462−1474

epitaxially on the underlying CdSe crystal.[45] In the case of InP on the other hand, the epitaxial growth of a metal sulfide shell can be more problematic since our work shows that S tends to form a suprastoichiometric surface termination that does not continue the crystal structure of the underlying InP crystal. This may explain why most successful InP-based core/shell synthesis protocols are either one-pot approaches or rely on an initial saturation of the InP surface with the cations such as Zn or Cd.[46−49]

In view of this spectrum of applications, the computational approach introduced here provides a consistent way to calculate adsorption energies under standardized conditions. Indeed, by considering a process where ligands are taken from a neutral reservoir and added to a neutral, nonstoichiometric crystal surface, addition energies can be calculated for any ligand, be it L-, X- or Z-type, relative to a predefined reference state without the upfront introduction of charged species. Although the calculated adsorption energy will depend on the choice of the reference state, this is less of an issue then it may seem even in the case of X-type ligands such as oleates, thiolates or phosphonates. Similar to the hydrogen chalcogenides studied here, an appropriate reference state for such ligands is the corresponding acid HX. In the case of addition to a Cd-rich CdSe surface, the first ligand addition energy $E^1_{\mathrm{add},X}$ thus corresponds to the reaction energy of a process where the X-type ligand is exchanged between the acid and the CdSe surface:

$$\mathrm{HX} + [\mathrm{CdSe}](\mathrm{Cd}) \rightarrow [\mathrm{CdSe}](\mathrm{CdX}) + \frac{1}{2}\mathrm{H_2} \quad (7)$$

Using the same notation, an exchange reaction where the ligand X is exchanged for X′ can then be written as

$$\mathrm{HX'} + [\mathrm{CdSe}](\mathrm{CdX}) \rightarrow [\mathrm{CdSe}](\mathrm{CdX'}) + \mathrm{HX} \quad (8)$$

Hence, the exchange reaction is the difference of the X′ and X addition reactions such that its reaction energy follows from the difference between the respective addition energies, a number that is independent of the choice of the hydrogen reference state. In the same way, the choice of reference state is not important if the binding of a particular ligand to different crystal surfaces is considered since also in this case, conclusions on preferential binding will follow from differences in ligand addition energy.

CONCLUSIONS

We have introduced the ligand addition energy as the energy change upon transferring a ligand from a reference reservoir to a solid surface and used it to analyze the stoichiometry of colloidal nanocrystals. Using the thermodynamic principle that ligand addition will stop when the ligand addition energy becomes endothermic, we determined the thermodynamically most stable surface composition of metal-rich CdSe, ZnSe and InP surfaces exposed to reservoirs of halogens, chalcogens or hydrochalcogens. In all cases, ligand addition energies were calculated with density-functional theory using periodic models of the solid surface. For the majority of the material/ligand combinations, ligand addition energies become endothermic once the surface composition complied with the so-called oxidation-number sum rule. This rule—supported by experimental observations—accounts for the nanocrystal composition by attributing to each constituent a charge equal to its most common oxidation state and requiring that the entire nanocrystal be charge neutral. Exceptions to the sum rule typically occurred for strongly electronegative ligands such as fluorine and oxygen and for the combination of InP with each of the chalcogens, where in all cases more ligands could be added than predicted by the sum rule. Only for sum-rule compliant systems we observe that the excess metal cations and the added ligands epitaxially extend the bulk crystal structure. With sum-rule defiant systems, ligands typically insert between cation−anion bonds, thereby oxidizing also the anion and inducing surface terminations that are not extensions of the bulk crystal. We conclude that the extension of the oxidation-number sum rule beyond the metal selenide and metal sulfide nanocrystals typically studied in the literature is not straightforward. However, the ligand addition energy introduced here provides an apt framework for the computational investigation of such systems. Moreover, the thermodynamic study of nanocrystals exposed to ligand reservoirs extends far beyond the analysis of the stoichiometry of metal-rich binary nanocrystals. Ligand addition energies can be similarly used to assess the stability of nanocrystals exposed to ambient conditions after synthesis or specific precursors during multistep synthetic procedures such as core/shell growth. In addition, they provide a consistent framework, based on well-known reference states, to compute adsorption energies of L-, X- and Z-type ligands and determine reaction energies of ligand exchange processes. As such, the ligand addition energy will be a most useful quantity for future computational studies on the structure, stability and reactivity of nanocrystal surfaces.

METHODS

Energetic calculations, both for slabs and crystalline reference states are performed with spin-polarized periodic density-functional theory using the Perdew−Burke−Ernzerhof (PBE) functional as implemented in the Vienna *Ab Initio* Simulation (VASP) package.[50−56] Charges were calculated using the periodic Hirschfeld-I scheme developed by Vanpoucke *et al.* as implemented for VASP in the HIVE software package.[57,58] Electron affinities and ionization potentials were determined using the high-accuracy benchmarking method CCSD(T) method through the Gaussian 09 package.[59−64]

Slab Models. Slab models were created from bulk crystals which were relaxed from experimental geometries obtained from the Crystallography Open Database (COD).[65,66] Properties of each slab model have been calibrated to minimize the remaining error on the initial adsorption energy to a maximum of 10 kJ/mol.[67] At this accuracy level the computational cost of the full screening procedure is approximately 300 coreyears. Calibrated settings can be separated into two categories: geometric and technical. Geometric settings include the number of atomic layers in the slab, the amount of layers kept fixed during ionic relaxation, the lateral size of the cell and the vacuum distance between slabs. Technical details include basis set size, density of the reciprocal and real-space sampling grids, core electron approximation and smearing method.

Results for the geometric calibration are shown in Table 2. Note that the number of layers mentioned in the table excludes the excess atoms. Slab models for CdSe are thinner and asymmetric, while zinc blende models contain a mirror plane in the center of the slab. In an asymmetric model dipole moments are created upon adsorption,

Table 2. Specification of the Slab Model

	CdSe	ZnSe	InP
surface	$(11\bar{2}0)$	(110)	(110)
# layers (excl. exc)	4	9	9
# fixed	2	5	5
vacuum (in nm)	3	2	2
ϵ_{slab}	1.43	1	1

DOI: 10.1021/acsnano.5b06965
ACS Nano 2016, 10, 1462−1474

Table 3. Technical Specifications

	relax, low	relax, high	static	DFT-PT
PAW projectors	normal	hard	hard	normal
E_{cut} (eV)	400	850	850	400
k mesh (wurtzite)	5 × 5 × 1	5 × 5 × 1	5 × 5 × 1	11 × 11 × 1
k mesh (zinc blende)	7 × 7 × 1	11 × 11 × 1	11 × 11 × 1	/
smearing	Gauss σ = 0.01	Gauss σ = 0.01	Tetra	Gauss σ = 0.001

causing additional interaction between the periodic copies of the slab. While it is a simple process to apply dipole corrections, they require calculation of the relative macroscopic dielectric constant ϵ_{slab} of the cell to properly take into account the screening of the interaction by the slab.[68−70] Both electronic and ionic contributions to ϵ_{slab} can be calculated with DFT perturbation theory (DFT-PT),[71,72] but at a steep computational cost. Since ϵ_{slab} does not vary significantly with the surface configuration it is sufficient to calculate it once for the desired slab thickness. The energy is corrected for all asymmetric slab calculations, effects on the potential are not corrected. In a symmetric model adsorption takes place simultaneously on both sides of the slab, in opposite directions, canceling out the surface dipole moments.[73] This double adsorption is the reason why symmetric slabs are thicker than their asymmetic counterparts, but symmetry can be exploited to reduce calculation time. During all ionic relaxations the two outer layers, together with excess atoms and ligands, were left free to relax. The other layers are kept fixed at the bulk lattice configuration in all cases. Vacuum distance was chosen to be minimally 2 nm in all cases, large enough to buffer any changes during relaxation and ensuring the potential is able to return to its vacuum level away from the slab. A larger vacuum of 3 nm is used for the CdSe cell to ensure the local potential is not significantly affected by the asymmetric surfaces.

The technical settings used for a specific calculation vary with its type. For each adsorption a lower accuracy relaxation is performed first, followed by a high accuracy relaxation and finally a high accuracy static calculation to refine the energies. These settings are the same for all three materials, except K-mesh, and are summarized in Table 3 together with the settings for the DFT-PT calculations used for CdSe. Core electrons are treated with the PAW projector method.[74,75] The default projector sets are used in most cases. For high accuracy calculations hard projector sets are used where available (O, S, F, Cl and P) as these are more accurate for molecular-like bonds which can exist at the surface. A plane wave basis set is used with a size determined by the plane wave energy cutoff E_{cut}. The high accuracy calculations used a higher E_{cut} for the hard projector sets. A different reciprocal grid is used for the wurtzite and zinc blende cells, but with both including the Γ point. The Monkhorst−Pack[76−78] sampling grid listed in the table is valid for the unit cell. For the InP supercell calculations the 11 sampling points along either the k_x or k_y direction were reduced to 7 when their corresponding real-space lattice parameters were doubled. Due to the inherently larger cell to represent the CdSe surface, the reciprocal grid density was lower and kept constant. Gaussian smearing is used during relaxations, with the static calculation using the tetrahedron method with Blöchl corrections[79] for accurate energies. DFT-PT calculations require a significantly denser reciprical grid to achieve convergence and a very low smearing width σ. To ensure no extra errors are induced PREC = Accurate is used in all cases, creating a denser real-space grid and the usage of real-space projectors[80] is explicitly disabled. Reference states were calculated using the same workflow and settings, but with a k-mesh density determined by VASP's auto mesh generation parameter l = 70. The bulk crystal calculations as prerequisite for the pristine slab used E_{cut} = 700 and 1100 eV for soft and hard potentials respectively to ensure minimal strain. The number of k-points sampled in the first Brillouin zone was 9261 for all three materials.

Electron Affinities and Ionization Potentials. These properties were determined based on nonperiodic calculations on single atoms. The electron affinity (EA) and ionization potential (IP) can be defined as follows:

$$\mathrm{EA} = \frac{E(N) - E(N+1)}{2} \tag{9}$$

$$\mathrm{IP} = \frac{E(N-1) - E(N)}{2} \tag{10}$$

where $E(N)$ is the energy of the system with N electrons. The energy in this case is calculated using CCSD(T) with the Def2-QZVPPD basis set as obtained from Basis Set Exchange.[81,82]

ASSOCIATED CONTENT

Supporting Information

The Supporting Information is available free of charge on the ACS Publications website at DOI: 10.1021/acsnano.5b06965.

An overview of the excess surface morphologies and associated charges; an example of ligand surface reactions; the suprastoichiometric adsorption of oxygen on InP for σ = 8/3; and surface morphologies for all data points shown in Figure 4. (PDF)

AUTHOR INFORMATION

Corresponding Authors

*E-mail: stefaan.cottenier@ugent.be.
*E-mail: zeger.hens@ugent.be.

Notes

The authors declare no competing financial interest.

ACKNOWLEDGMENTS

Z.H., S.C., and V.V.S. acknowledge the Research Foundation Flanders (FWO-Vlaanderen) for funding (Project. No. G.0760.12). Z.H. acknowledges support by the European Comission *via* the Marie-Sklodowska Curie action Phonsi (H2020-MSCA-ITN-642656), the Belgian Science Policy office (IAP 7.35, photonics@be) and Ghent University (GOA 01G01513). The computational resources and services used in this work were provided by the VSC (Flemish Supercomputer Center), funded by the Hercules Foundation and the Flemish Government - department EWI. S.C. acknowledges financial support from OCAS NV by an OCAS-endowed chair at Ghent University. V.V.S. acknowledges the Research Board of Ghent University for funding.

REFERENCES

(1) Murray, C.; Kagan, C.; Bawendi, M. Synthesis and Characterization of Monodisperse Nanocrystals and Close-Packed Nanocrystal Assemblies. *Annu. Rev. Mater. Sci.* **2000**, *30*, 545−610.
(2) Yin, Y.; Alivisatos, A. Colloidal Nanocrystal Synthesis and the Organic-Inorganic Interface. *Nature* **2005**, *437*, 664−670.
(3) Talapin, D. V.; Lee, J.-S.; Kovalenko, M. V.; Shevchenko, E. V. Prospects of Colloidal Nanocrystals for Electronic and Optoelectronic Applications. *Chem. Rev.* **2010**, *110*, 389−458.
(4) Owen, J. S.; Park, J.; Trudeau, P.-E.; Alivisatos, A. P. Reaction Chemistry and Ligand Exchange at Cadmium-Selenide Nanocrystal Surfaces. *J. Am. Chem. Soc.* **2008**, *130*, 12279−12281.

DOI: 10.1021/acsnano.5b06965
ACS Nano 2016, 10, 1462−1474

(5) Anderson, N. C.; Owen, J. S. Soluble, Chloride-Terminated CdSe Nanocrystals: Ligand Exchange Monitored by H-1 and P-31 NMR Spectroscopy. *Chem. Mater.* **2013**, *25*, 69−76.
(6) De Roo, J.; Van den Broeck, F.; De Keukeleere, K.; Martins, J. C.; Van Driessche, I.; Hens, Z. Unravelling the Surface Chemistry of Metal Oxide Nanocrystals, the Role of Acids and Bases. *J. Am. Chem. Soc.* **2014**, *136*, 9650−9657.
(7) Dierick, R.; Van den Broeck, F.; De Nolf, K.; Zhao, Q.; Vantomme, A.; Martins, J. C.; Hens, Z. Surface Chemistry of $CuInS_2$ Colloidal Nanocrystals, Tight Binding of L-Type Ligands. *Chem. Mater.* **2014**, *26*, 5950−5957.
(8) Moreels, I.; Lambert, K.; De Muynck, D.; Vanhaecke, F.; Poelman, D.; Martins, J. C.; Allan, G.; Hens, Z. Composition and Size-Dependent Extinction Coefficient of Colloidal PbSe Quantum Dots. *Chem. Mater.* **2007**, *19*, 6101−6106.
(9) Fritzinger, B.; Capek, R. K.; Lambert, K.; Martins, J. C.; Hens, Z. Utilizing Self-Exchange To Address the Binding of Carboxylic Acid Ligands to CdSe Quantum Dots. *J. Am. Chem. Soc.* **2010**, *132*, 10195−10201.
(10) Moreels, I.; Justo, Y.; De Geyter, B.; Haustraete, K.; Martins, J. C.; Hens, Z. Size-Tunable, Bright, and Stable PbS Quantum Dots: A Surface Chemistry Study. *ACS Nano* **2011**, *5*, 2004−2012.
(11) Kamal, J. S.; Omari, A.; Van Hoecke, K.; Zhao, Q.; Vantomme, A.; Vanhaecke, F.; Capek, R. K.; Hens, Z. Size-Dependent Optical Properties of Zinc Blende Cadmium Telluride Quantum Dots. *J. Phys. Chem. C* **2012**, *116*, 5049−5054.
(12) Gomes, R.; Hassinen, A.; Szczygiel, A.; Zhao, Q.; Vantomme, A.; Martins, J. C.; Hens, Z. Binding of Phosphonic Acids to CdSe Quantum Dots: A Solution NMR Study. *J. Phys. Chem. Lett.* **2011**, *2*, 145−152.
(13) Hassinen, A.; Gomes, R.; De Nolf, K.; Zhao, Q.; Vantomme, A.; Martins, J. C.; Hens, Z. Surface Chemistry of CdTe Quantum Dots Synthesized in Mixtures of Phosphonic Acids and Amines: Formation of a Mixed Ligand Shell. *J. Phys. Chem. C* **2013**, *117*, 13936−13943.
(14) Anderson, N. C.; Hendricks, M. P.; Choi, J. J.; Owen, J. S. Ligand Exchange and the Stoichiometry of Metal Chalcogenide Nanocrystals: Spectroscopic Observation of Facile Metal-Carboxylate Displacement and Binding. *J. Am. Chem. Soc.* **2013**, *135*, 18536−18548.
(15) Green, M. A New Approach to the Formal Classificaton of Covalent Compounds of the Elements. *J. Organomet. Chem.* **1995**, *500*, 127−148.
(16) Zherebetskyy, D.; Scheele, M.; Zhang, Y.; Bronstein, N.; Thompson, C.; Britt, D.; Salmeron, M.; Alivisatos, P.; Wang, L.-W. Hydroxylation of the Surface of PbS Nanocrystals Passivated with Oleic Acid. *Science* **2014**, *344*, 1380−1384.
(17) Sandeep, C. S. S.; Azpiroz, J. M.; Evers, W. H.; Boehme, S.-C.; Moreels, I.; Kinge, S.; Siebbeles, L. D. A.; Infante, I.; Houtepen, A. J. Epitaxially Connected PbSe Quantum-Dot Films: Controlled Neck Formation and Optoelectronic Properties. *ACS Nano* **2014**, *8*, 11499−11511.
(18) Pilania, G.; Sadowski, T.; Ramprasad, R. Oxygen Adsorption on CdSe Surfaces: Case Study of Asymmetric Anisotropic Growth through Ab Initio Computations. *J. Phys. Chem. C* **2009**, *113*, 1863−1871.
(19) Rempel, J. Y.; Trout, B. L.; Bawendi, M. G.; Jensen, K. F. Density Functional Theory Study of Ligand Binding on CdSe (0001), $(000\bar{1})$, and $(11\bar{2}0)$ Single Crystal Relaxed and Reconstructed Surfaces: Implications for Nanocrystalline Growth. *J. Phys. Chem. B* **2006**, *110*, 18007−18016.
(20) Manna, L.; Wang, L.; Cingolani, R.; Alivisatos, A. P. First-Principles Modeling of Unpassivated and Surfactant-Passivated Bulk Facets of Wurtzite CdSe: A Model System for Studying the Anisotropic Growth of CdSe Nanocrystals. *J. Phys. Chem. B* **2005**, *109*, 6183−6192.
(21) Gao, Y.; Zhou, B.; Kang, S.-g.; Xin, M.; Yang, P.; Dai, X.; Wang, Z.; Zhou, R. Effect of Ligands on the Characteristics of $(CdSe)_{13}$ Quantum Dots. *RSC Adv.* **2014**, *4*, 27146−27151.
(22) Kuznetsov, A. E.; Beratan, D. N. Structural and Electronic Properties of Bare and Capped $Cd_{33}Se_{33}$ and $Cd_{33}Te_{33}$ Quantum Dots. *J. Phys. Chem. C* **2014**, *118*, 7094−7109.
(23) Nadler, R.; Sanz, J. F. Simulating the Optical Properties of CdSe Clusters Using the RT-TDDFT Approach. *Theor. Chem. Acc.* **2013**, *132*, 1342.
(24) Yang, P.; Tretiak, S.; Ivanov, S. Influence of Surfactants and Charges on CdSe Quantum Dots. *J. Cluster Sci.* **2011**, *22*, 405−431.
(25) Xu, S.; Wang, C.; Cui, Y. Theoretical Investigation of CdSe Clusters: Influence of Solvent and Ligand on Nanocrystals. *J. Mol. Model.* **2010**, *16*, 469−473.
(26) Xu, S.; Wang, C.; Cui, Y. Theoretical Investigation for ZnSe Clusters: Influence of Solvent and Ligand on their Characteristics. *J. Mol. Struct.: THEOCHEM* **2009**, *916*, 168−171.
(27) Yang, P.; Tretiak, S.; Masunov, A. E.; Ivanov, S. Quantum Chemistry of the Minimal CdSe Clusters. *J. Chem. Phys.* **2008**, *129*, 074709.
(28) Liu, W.; Zheng, W. T.; Jiang, Q. First-Principles Study of the Surface Energy and Work Function of III-V Semiconductor Compounds. *Phys. Rev. B: Condens. Matter Mater. Phys.* **2007**, *75*, 235322.
(29) Tsai, M.-H.; Dow, J. D.; Wang, R. P.; Kasowski, R. V. Relaxation of Zinc-Blende (110) Surfaces. *Phys. Rev. B: Condens. Matter Mater. Phys.* **1989**, *40*, 9818−9823.
(30) Holec, D.; Mayrhofer, P. H. Surface Energies of AlN Allotropes from First Principles. *Scr. Mater.* **2012**, *67*, 760−762.
(31) Mulliken, R. S. Electronic Structures of Polyatomic Molecules and Valence. V. Molecules RX_n. *J. Chem. Phys.* **1933**, *1*, 492−503.
(32) Furtado, J.; De Proft, F.; Geerlings, P. The Noble Gases: How Their Electronegativity and Hardness Determines Their Chemistry. *J. Phys. Chem. A* **2015**, *119*, 1339−1346.
(33) Geerlings, P.; De Proft, F.; Langenaeker, W. Conceptual Density Functional Theory. *Chem. Rev.* **2003**, *103*, 1793−1874.
(34) Pearson, R. G. Hard and Soft Acids and Bases, HSAB, part 1: Fundamental Principles. *J. Chem. Educ.* **1968**, *45*, 581−587.
(35) Pearson, R. G. Hard and Soft Acids and Bases, HSAB, part II: Underlying Theories. *J. Chem. Educ.* **1968**, *45*, 643−648.
(36) Pearson, R. G. The HSAB Principle. In *Chemical Hardness*; Wiley-VCH Verlag GmbH & Co. KGaA, 2005; pp 1−27.
(37) Battaglia, D.; Peng, X. Formation of High Quality InP and InAs Nanocrystals in a Noncoordinating Solvent. *Nano Lett.* **2002**, *2*, 1027−1030.
(38) Xie, R.; Battaglia, D.; Peng, X. Colloidal InP Nanocrystals as Efficient Emitters Covering Blue to Near-Infrared. *J. Am. Chem. Soc.* **2007**, *129*, 15432−15433.
(39) Cros-Gagneux, A.; Delpech, F.; Nayral, C.; Cornejo, A.; Coppel, Y.; Chaudret, B. Surface Chemistry of InP Quantum Dots: A Comprehensive Study. *J. Am. Chem. Soc.* **2010**, *132*, 18147−18157.
(40) Flamee, S.; Cirillo, M.; Abe, S.; De Nolf, K.; Gomes, R.; Aubert, T.; Hens, Z. Fast, High Yield, and High Solid Loading Synthesis of Metal Selenide Nanocrystals. *Chem. Mater.* **2013**, *25*, 2476−2483.
(41) Kim, M. R.; Miszta, K.; Povia, M.; Brescia, R.; Christodoulou, S.; Prato, M.; Marras, S.; Manna, L. Influence of Chloride Ions on the Synthesis of Colloidal Branched CdSe/CdS Nanocrystals by Seeded Growth. *ACS Nano* **2012**, *6*, 11088−11096.
(42) Lim, J.; Bae, W. K.; Park, K. U.; zur Borg, L.; Zentel, R.; Lee, S.; Char, K. Controlled Synthesis of CdSe Tetrapods with High Morphological Uniformity by the Persistent Kinetic Growth and the Halide-Mediated Phase Transformation. *Chem. Mater.* **2013**, *25*, 1443−1449.
(43) Meyns, M.; Iacono, F.; Palencia, C.; Geweke, J.; Coderch, M. D.; Fittschen, U. E. A.; Gallego, J. M.; Otero, R.; Juarez, B. H.; Klinke, C. Shape Evolution of CdSe Nanoparticles Controlled by Halogen Compounds. *Chem. Mater.* **2014**, *26*, 1813−1821.
(44) Li, J.; Wang, Y.; Guo, W.; Keay, J.; Mishima, T.; Johnson, M.; Peng, X. Large-Scale Synthesis of Nearly Monodisperse CdSe/CdS Core/Shell Nanocrystals Using Air-Stable Reagents *via* Successive Ion Layer Adsorption and Reaction. *J. Am. Chem. Soc.* **2003**, *125*, 12567−12575.

DOI: 10.1021/acsnano.5b06965
ACS Nano 2016, 10, 1462−1474

(45) Tschirner, N.; Lange, H.; Schliwa, A.; Biermann, A.; Thomsen, C.; Lambert, K.; Gomes, R.; Hens, Z. Interfacial Alloying in CdSe/CdS Heteronanocrystals: A Raman Spectroscopy Analysis. *Chem. Mater.* **2012**, *24*, 311−318.
(46) Li, L.; Reiss, P. One-Pot Synthesis of Highly Luminescent InP/ZnS Nanocrystals Without Precursor Injection. *J. Am. Chem. Soc.* **2008**, *130*, 11588−11589.
(47) Xu, S.; Ziegler, J.; Nann, T. Rapid Synthesis of Highly Luminescent InP and InP/ZnS Nanocrystals. *J. Mater. Chem.* **2008**, *18*, 2653−2656.
(48) Dennis, A. M.; Mangum, B. D.; Piryatinski, A.; Park, Y.-S.; Hannah, D. C.; Casson, J. L.; Williams, D. J.; Schaller, R. D.; Htoon, H.; Hollingsworth, J. A. Suppressed Blinking and Auger Recombination in Near-Infrared Type-II InP/CdS Nanocrystal Quantum Dots. *Nano Lett.* **2012**, *12*, 5545−5551.
(49) Tessier, M. D.; Dupont, D.; De Nolf, K.; De Roo, J.; Hens, Z. Economic and Size-Tunable Synthesis of InP/ZnE (E = S, Se) Colloidal Quantum Dots. *Chem. Mater.* **2015**, *27*, 4893−4898.
(50) Kresse, G.; Furthmüller, J. Efficiency of Ab-Initio Total Energy Calculations for Metals and Semiconductors Using a Plane-Wave Basis Set. *Comput. Mater. Sci.* **1996**, *6*, 15−50.
(51) Kresse, G.; Furthmüller, J. Efficient Iterative Schemes for Ab Initio Total-Energy Calculations Using a Plane-Wave Basis Set. *Phys. Rev. B: Condens. Matter Mater. Phys.* **1996**, *54*, 11169−11186.
(52) Kresse, G.; Hafner, J. Ab Initio Molecular-Dynamics Simulation of the Liquid-Metal-Amorphous-Semiconductor Transition in Germanium. *Phys. Rev. B: Condens. Matter Mater. Phys.* **1994**, *49*, 14251−14269.
(53) Kresse, G.; Hafner, J. Ab Initio Molecular Dynamics for Liquid Metals. *Phys. Rev. B: Condens. Matter Mater. Phys.* **1993**, *47*, 558.
(54) Perdew, J. P.; Burke, K.; Ernzerhof, M. Erratum: Generalized Gradient Approximation Made Simple. *Phys. Rev. Lett.* **1997**, *78*, 1396.
(55) Perdew, J. P.; Burke, K.; Ernzerhof, M. Generalized Gradient Approximation Made Simple. *Phys. Rev. Lett.* **1996**, *77*, 3865−3868.
(56) Stroppa, A.; Kresse, G. The Shortcomings of Semi-Local and Hybrid Functionals: What We Can Learn from Surface Science Studies. *New J. Phys.* **2008**, *10*, 063020.
(57) Vanpoucke, D. E. P.; Bultinck, P.; Van Driessche, I. Extending Hirshfeld-I to Bulk and Periodic Materials. *J. Comput. Chem.* **2013**, *34*, 405−417.
(58) Vanpoucke, D. E. P.; Van Driessche, I.; Bultinck, P. Reply to Comment on Extending Hirshfeld-I to Bulk and Periodic Materials. *J. Comput. Chem.* **2013**, *34*, 422−427.
(59) Frisch, M. J.; Trucks, G. W.; Schlegel, H. B.; Scuseria, G. E.; Robb, M. A.; Cheeseman, J. R.; Scalmani, G.; Barone, V.; Mennucci, B.; Petersson, G. A.; et al.*et al. Gaussian09*, Revision D.01; Gaussian Inc.: Wallingford, CT, 2009.
(60) Bartlett, R. J.; Purvis, G. D. Many-body Perturbation Theory, Coupled-Pair Many-Electron Theory, and the Importance of Quadruple Excitations for the Correlation Problem. *Int. J. Quantum Chem.* **1978**, *14*, 561−581.
(61) Purvis, G. D.; Bartlett, R. J. A Full Coupled-Cluster Singles and Doubles Model: The Inclusion of Disconnected Triples. *J. Chem. Phys.* **1982**, *76*, 1910−1918.
(62) Pople, J. A.; HeadGordon, M.; Raghavachari, K. Quadratic Configuration Interaction. A General Technique for Determining Electron Correlation Energies. *J. Chem. Phys.* **1987**, *87*, 5968−5975.
(63) Raghavachari, K.; Trucks, G. W.; Pople, J. A.; Head-Gordon, M. A Fifth-Order Perturbation Comparison of Electron Correlation Theories. *Chem. Phys. Lett.* **1989**, *157*, 479−483.
(64) Lee, T. J.; Rendell, A. P.; Taylor, P. R. Comparison of the Quadratic Configuration Interaction and Coupled-Cluster Approaches to Electron Correlation Including the Effect of Triple Excitations. *J. Phys. Chem.* **1990**, *94*, 5463−5468.
(65) Gražulis, S.; Chateigner, D.; Downs, R. T.; Yokochi, A. F. T.; Quirós, M.; Lutterotti, L.; Manakova, E.; Butkus, J.; Moeck, P.; Le Bail, A. Crystallography Open Database (COD): an Open-Access Collection of Crystal Structures and Platform for World-Wide Collaboration. *Nucleic Acids Res.* **2012**, *40*, D420−D427.
(66) Gražulis, S.; Chateigner, D.; Downs, R. T.; Yokochi, A. F. T.; Quirós, M.; Lutterotti, L.; Manakova, E.; Butkus, J.; Moeck, P.; Le Bail, A. Crystallography Open Database - an Open-Access Collection of Crystal Structures. *J. Appl. Crystallogr.* **2009**, *42*, 726−729.
(67) Singh-Miller, N. E.; Marzari, N. Surface Energies, Work Functions, and Surface Relaxations of Low-Index Metallic Surfaces from First Principles. *Phys. Rev. B: Condens. Matter Mater. Phys.* **2009**, *80*, 235407.
(68) Makov, G.; Payne, M. C. Periodic Boundary-Conditions in Ab-Initio Calculations. *Phys. Rev. B: Condens. Matter Mater. Phys.* **1995**, *51*, 4014−4022.
(69) Neugebauer, J.; Scheffler, M. Adsorbate-Substrate and Adsorbate-Adsorbate Interactions of Na and K Adlayers on Al(111). *Phys. Rev. B: Condens. Matter Mater. Phys.* **1992**, *46*, 16067−16080.
(70) Eichler, A.; Kresse, G. First-Principles Calculations for the Surface Termination of Pure and Yttria-Doped Zirconia Surfaces. *Phys. Rev. B: Condens. Matter Mater. Phys.* **2004**, *69*, 045402.
(71) Gajdoš, M.; Hummer, K.; Kresse, G.; Furthmüller, J.; Bechstedt, F. Linear Optical Properties in the Projector-Augmented Wave Methodology. *Phys. Rev. B: Condens. Matter Mater. Phys.* **2006**, *73*, 045112.
(72) Baroni, S.; Resta, R. Ab Initio Calculation of the Macroscopic Dielectric Constant in Silicon. *Phys. Rev. B: Condens. Matter Mater. Phys.* **1986**, *33*, 7017−7021.
(73) Joos, L.; Filot, I. A. W.; Cottenier, S.; Hensen, E. J. M.; Waroquier, M.; Speybroeck, V. V.; van Santen, R. A. Reactivity of CO on Carbon-Covered Cobalt Surfaces in Fischer−Tropsch Synthesis. *J. Phys. Chem. C* **2014**, *118*, 5317−5327.
(74) Kresse, G.; Joubert, D. From Ultrasoft Pseudopotentials to the Projector Augmented-Wave Method. *Phys. Rev. B: Condens. Matter Mater. Phys.* **1999**, *59*, 1758.
(75) Blöchl, P. E. Projector Augmented-Wave Method. *Phys. Rev. B: Condens. Matter Mater. Phys.* **1994**, *50*, 17953.
(76) Monkhorst, H. J.; Pack, J. D. Special Points for Brillouin-Zone Integrations. *Phys. Rev. B* **1976**, *13*, 5188−5192.
(77) Chadi, D. J.; Cohen, M. L. Special Points in the Brillouin Zone. *Phys. Rev. B* **1973**, *8*, 5747−5753.
(78) Baldereschi, A. Mean-Value Point in the Brillouin Zone. *Phys. Rev. B* **1973**, *7*, 5212−5215.
(79) Blöchl, P. E.; Jepsen, O.; Andersen, O. K. Improved Tetrahedron Method for Brillouin-Zone Integrations. *Phys. Rev. B: Condens. Matter Mater. Phys.* **1994**, *49*, 16223−16233.
(80) King-Smith, R. D.; Payne, M. C.; Lin, J. S. Real-Space Implementation of Nonlocal Pseudopotentials for First-Principles Total-Energy Calculations. *Phys. Rev. B: Condens. Matter Mater. Phys.* **1991**, *44*, 13063−13066.
(81) Feller, D. The Role of Databases in Support of Computational Chemistry Calculations. *J. Comput. Chem.* **1996**, *17*, 1571−1586.
(82) Schuchardt, K. L.; Didier, B. T.; Elsethagen, T.; Sun, L.; Gurumoorthi, V.; Chase, J.; Li, J.; Windus, T. L. Basis Set Exchange: A Community Database for Computational Sciences. *J. Chem. Inf. Model.* **2007**, *47*, 1045−1052.

DOI: 10.1021/acsnano.5b06965
ACS Nano 2016, 10, 1462−1474